

# Physics-Constrained Hardware-Efficient Ansatz on Quantum Computers that is Universal, Systematically Improvable, and Size-consistent

Xiaoxiao Xiao<sup>1</sup>, Hewang Zhao<sup>1</sup>, Jiajun Ren<sup>1</sup>, Wei-Hai Fang<sup>1</sup>, and Zhendong Li<sup>1,\*</sup>

<sup>1</sup>Key Laboratory of Theoretical and Computational Photochemistry, Ministry of Education, College of Chemistry, Beijing Normal University, Beijing 100875, China

\*corresponding author(s): Zhendong Li (zhendongli@bnu.edu.cn)

## ABSTRACT

Variational wavefunction ansätze are at the heart of solving quantum many-body problems in physics and chemistry. Here, we propose a physics-constrained approach for designing hardware-efficient ansatz (HEA) with rigorous theoretical guarantees on quantum computers by satisfying a few fundamental constraints, which is inspired by the remarkably successful way to design exchange-correlation functionals in density functional theories by satisfying exact constraints. Specifically, we require that the target HEA to be universal, systematically improvable, and size-consistent, which is an important concept in quantum many-body theories for scalability, but has been largely overlooked in previous designs of HEA by heuristics. We extend the notion of size-consistency to HEA, and present a concrete realization of HEA that satisfies all these fundamental constraints and only requires linear qubit connectivity. The developed physics-constrained HEA is superior to other heuristically designed HEA in terms of both accuracy and scalability, as demonstrated numerically for the Heisenberg model and some typical molecules. In particular, we find that restoring size-consistency can significantly reduce the number of layers needed to reach certain accuracy. In contrast, the failure of other HEA to satisfy these constraints severely limits their scalability to larger systems with more than ten qubits. Our work highlights the importance of incorporating physical constraints into the design of HEA for efficiently solving many-body problems on quantum computers.

# Introduction

Efficient simulation of quantum many-body problems is an enduring frontier in computational physics and chemistry<sup>1</sup>. Among many different approaches, the variational method represents a powerful and versatile technique to tackle quantum many-body problems. A wealth of variational wavefunction ansätze on classical computers have been developed over the past decades. Prominent examples include Slater determinants, Gutzwiller wavefunction<sup>2</sup>, Jastrow wavefunction<sup>3</sup>, tensor network states<sup>4–10</sup>, and neural network states<sup>11–17</sup>. Thanks to the rapid progress on quantum hardware<sup>18,19</sup>, the variational quantum eigensolver (VQE)<sup>20,21</sup>, which is a hybrid quantum-classical approach for solving quantum many-body problems<sup>22</sup>, has attracted much attention<sup>23–26</sup>. The central component of VQE is the preparation of a trial wavefunction on quantum computers, which ultimately determines the accuracy of the variational computation. However, compared to the development of variational ansätze on classical computers, the exploration of wavefunction ansätze on quantum computers is still in its infancy.

The available variational ansätze on quantum computers developed so far can be broadly classified into two categories: physics/chemistry-inspired and hardware-efficient ansätze, each with its own advantages and disadvantages. The unitary coupled cluster (UCC) ansatz<sup>27</sup> is the first ansatz proposed for determining molecular ground states on quantum computers<sup>20</sup>, which is motivated by the great success of the traditional coupled cluster theory on classical computers<sup>28</sup>. However, it quickly becomes impractical for large molecules on the current noisy intermediate-scale quantum (NISQ) hardware<sup>29</sup>, since the circuit depth scales as  $O(N^4)$  with respect to the number of qubits  $N$ <sup>30–32</sup>. Efforts have been devoted to reduce the complexity of UCC, resulting in many descendants of UCC such as the unitary paired CC ansatz<sup>33</sup>, the unitary cluster Jastrow ansatz<sup>34</sup>, and several adaptive variants<sup>35–38</sup>. Another type of physics-inspired ansatz is the Hamiltonian variational ansatz (HVA)<sup>39,40</sup>, which is problem specific and widely used for model systems<sup>41</sup>. When applied to general cases such as the molecular Hamiltonian in quantum chemistry, it suffers from the same problem as UCC.

Hardware efficient ansätze (HEA)<sup>42</sup>, proposed as a more practical alternative on near-term quantum

devices, take the following form

$$|\Psi\rangle = U_L(\vec{\theta}_L) \cdots U_1(\vec{\theta}_1) |\Phi_0\rangle \triangleq \prod_{l=1}^L U_l(\vec{\theta}_l) |\Phi_0\rangle, \quad (1)$$

where  $|\Phi_0\rangle$  is a reference state and the repeating unit  $U_l(\vec{\theta}_l)$  is a parameterized quantum circuit composed of gates that are native on quantum hardware<sup>42</sup>, such as single-qubit rotation gates and two-qubit entangling gates (see Fig. 1a). Given the hardware constraints, there is still a great deal of freedom in choosing the layout of the circuit block  $U_l(\vec{\theta}_l)$ . So far, the architectures of HEA have been designed mostly by heuristics, and there is no theoretical guarantee for their performance. Furthermore, the optimization of HEA is challenging<sup>43</sup> as the number of qubits  $N$  and the number of layers  $L$  increases, due to the proliferation of low-quality local minima<sup>44</sup> and the exponential vanishing of gradients, known as the 'barren plateau' phenomenon<sup>45</sup>. These problems severely limit the scalability of HEA beyond small systems. Therefore, it is highly desirable to design a variational ansatz with rigorous theoretical basis, while at the same time being hardware-efficient on near-term devices<sup>46,47</sup>.

In this work, we present a way to design HEA with rigorous theoretical properties by imposing fundamental constraints. This is inspired by the remarkably successful way to design exchange-correlation (XC) functionals in density functional theories (DFT) by requiring the XC functionals to satisfy exact constraints<sup>48</sup>, which has lead to reliable non-empirical XC functionals for a wide range of systems<sup>49,50</sup>. The remaining part of the paper is organized as follows: First, we introduce four fundamental constraints for HEA. Specifically, we require the ansatz to be universal, systematically improvable, and size-consistent (or multiplicatively separable), which is an important property for scalability in quantum many-body theory. Then, we present an HEA, termed as physics-constrained HEA, which satisfies all these requirements and requires only linear qubit connectivity with nearest neighbor interactions. The effectiveness of this ansatz is demonstrated for the Heisenberg model and some typical molecules. The comparison with other HEA shows that incorporating physical constraints into the design of HEA is a promising way to design efficient and scalable variational ansatz on quantum computers.

## Results

### Fundamental constraints for HEA

We first introduce four fundamental constraints that a good HEA should satisfy, and then construct a concrete HEA that satisfies these constraints. Given a system  $A$ , suppose the variational space of HEA with  $L$  layers in Eq. (1) is denoted by  $V_A^L$ , we introduce the following four basic constraints for the possible form of  $U_l(\vec{\theta}_l)$ :

(1) *Universality*: any quantum state should be approximated arbitrarily well by the designed HEA with a sufficiently large number of layers  $L$ .

(2) *Systematic improvability*:  $V_A^L$  should be included in  $V_A^{L+1}$  for any  $L$ , i.e.  $V_A^L \subseteq V_A^{L+1}$ . This guarantees that the variational space is systematically expanded, and the variational energy converges monotonically as  $L$  increases, i.e.  $E_A^{L+1} \leq E_A^L$ . A simple sufficient condition for the systematic improvability is that there exists a set of parameters  $\vec{\theta}_l$  such that  $U_l(\vec{\theta}_l) = I$ .

(3) *Size-consistency*: since the exact wavefunction of a compound system  $A + B$  consisting of two noninteracting subsystems  $A$  and  $B$  is multiplicatively separable, i.e.  $|\Psi^{AB}\rangle = |\Psi^A\rangle|\Psi^B\rangle$ , we require that  $V_A^L \otimes V_B^L$  should be included in  $V_{A+B}^L$  for any  $L$ , i.e.  $V_A^L \otimes V_B^L \subseteq V_{A+B}^L$  (see Fig. 1b). As the Hamiltonian of the composite system is  $\hat{H}_{A+B} = \hat{H}_A + \hat{H}_B$ , the constraint ensures that the variational energy  $E_{A+B}^L$  of the composite system will not be worse than the sum of the individually computed energies  $E_A^L + E_B^L$ , i.e.  $E_{A+B}^L \leq E_A^L + E_B^L$ . This size-consistency condition requires that for any  $U_A(\vec{\theta}_{l,A})$  and  $U_B(\vec{\theta}_{l,B})$ , there exists a set of parameters  $\vec{\theta}_{l,A+B}$  such that  $U_{A+B}(\vec{\theta}_{l,A+B}) = U_A(\vec{\theta}_{l,A}) \otimes U_B(\vec{\theta}_{l,B})$ .

(4) *Noninteracting limit*: in the limit that all the qubits are noninteracting, the eigenstates are given by product states. We require that for a good HEA,  $L = 1$  should be sufficient for represent any product state, and hence  $L > 1$  is only required for entangled states.

As shown in Fig. 1b, the two inclusion constraints (2) and (3) represent the constraints for extending HEA in two different directions of quantum circuits. The size-consistency constraint (3) introduced for HEA extends the notion of size-consistency/size-extensivity in quantum chemistry<sup>51–53</sup> for the qualification and differentiation of many-body methods. A size-extensive method such as the coupled cluster theory<sup>52</sup> can provide energies that grow linearly with the number of electrons in the system. This is mandatory

for the application of a many-body method to large systems such as solids, because it guarantees that the quality of the energy will not deteriorate compared to that for small systems. This concept is therefore also essential for the scalability of the variational ansatz on quantum computers.

Some previously designed HEA by heuristics shown in Fig. 1a, including the commonly adopted  $R_y$  and  $R_y R_z$  (EfficientSU2) ansätze with different entangling blocks<sup>42</sup>, clearly fail to meet these important requirements, in particular, constraints (2) and (3). Besides, the HVA for model systems of the form  $U_l(\vec{\theta}_l) = \prod_k e^{i\theta_{l,k}\hat{H}_k}$ , where  $\hat{H}_k$  is a component of the Hamiltonian of the system  $\hat{H} = \sum_k \hat{H}_k$ , satisfies constraints (2) and (3), but does not necessarily meet constraints (1) and (4), which are requirements for general-purpose HEA. Finally, apart from these theoretical constraints, since most of existing quantum devices have restricted qubit connectivity, an additional hardware constraint is that the building block  $U_l(\vec{\theta}_l)$  should be easily implemented on quantum devices with restricted connectivity.

## Physics-constrained HEA

Just as the exact constraints do not uniquely determine the form of the XC functionals in DFT<sup>48</sup>, the above requirements still leave a lot of degree of freedom in the design of HEA. Here we propose one possible HEA that satisfies these basic requirements and only requires linear qubit connectivity, termed as physics-constrained HEA. Our starting point is the wavefunction given by a product of exponential of Pauli operators

$$|\Psi\rangle = e^{i\theta_L P_L} \dots e^{i\theta_1 P_1} |\Phi_0\rangle \triangleq \prod_{l=1}^L e^{i\theta_l P_l} |\Phi_0\rangle. \quad (2)$$

If one can choose all possible  $P_l \in \{I, X, Y, Z\}^{\otimes N}$ , this form of  $U_l(\theta_l) = e^{i\theta_l P_l}$  is universal<sup>54,55</sup>. It is also systematically improvable because the choice  $\theta_l = 0$  gives an identity operator. However, it does not satisfy constraints (3) and (4). Thus, if each layer of HEA has the ability to represent any  $e^{i\theta_l P_l}$  with  $P_l \in \{I, X, Y, Z\}^{\otimes N}$ , the resulting ansatz will automatically satisfy constraints (1) and (2), and we only need to modify it to satisfy constraints (3) and (4). The fact that any  $e^{i\theta_l P_l}$  can be represented by a quantum circuit with CNOT 'staircases'<sup>54</sup> motivates us to design  $U_l(\vec{\theta}_l)$  with a similar structure (see Fig. 1b with gates in white colors), where the forms of the single-qubit gates  $U_1$  and two-qubit gates  $U_2$  remain to be specified. We find the following sufficient condition for representing any  $e^{i\theta_l P_l}$  by the circuit block in Fig.

1b:

**Theorem 1.** *If  $U_2$  include gates in  $\{I, \text{CNOT}, \text{SWAP or iSWAP}\}$ , then the circuit block in Fig. 1b can represent any  $e^{i\theta_l P_l}$  with  $P_l \in \{I, Z\}^{\otimes N}$ . Furthermore, if  $U_1$  include gates in  $\{I, R_x(\pi/2), R_y(-\pi/2) \text{ or } H\}$ , then the circuit block can represent any  $e^{i\theta_l P_l}$  with  $P_l \in \{I, X, Y, Z\}^{\otimes N}$ .*

The proof is delegated into Methods section. We remark that the role of SWAP can be replaced by iSWAP, which is easier to implement on some quantum computing platforms, such as superconducting quantum devices<sup>56</sup>. There are still infinitely many ways to parameterize  $U_1$  and  $U_2$  that satisfy this sufficient condition, since a general single-qubit (two-qubit) gate can be described by three (fifteen) parameters, and at most three CNOT gates are needed for general two-qubit gates<sup>57,58</sup>. To minimize the number of parameters per circuit block and reduce the number of native two-qubit gates in  $U_2$ , here we present a parameterization of  $U_2$  with two parameters

$$U_2(\theta, \phi) = [I \otimes R_y(\phi/2)] U_{\text{fSim}}(\theta, \phi) [I \otimes R_y(-\phi/2)], \quad (3)$$

using the fSim gate  $U_{\text{fSim}}(\theta, \phi)$  native on some superconducting devices<sup>59</sup>

$$U_{\text{fSim}}(\theta, \phi) = \begin{bmatrix} 1 & 0 & 0 & 0 \\ 0 & \cos \theta & -i \sin \theta & 0 \\ 0 & -i \sin \theta & \cos \theta & 0 \\ 0 & 0 & 0 & e^{-i\phi} \end{bmatrix}, \quad (4)$$

which yields  $U_2(0, 0) = I$ ,  $U_2(-\pi/2, 0) = \text{iSWAP}$ , and  $U_2(0, \pi) = \text{CNOT}$ . A simple choice for the single-qubit gates  $U_1$  to satisfy the sufficient condition is

$$U_1(\theta, \phi) = R_x(\theta) R_y(\phi). \quad (5)$$

Eqs. (3) and (5) completely define a HEA, which can implement an exponential of any Pauli operator by appropriate choice of parameters. We will refer to it as XYZ1F in the following context, as an abbreviation for the combination of the three types of single-qubit rotation gates used and the two-qubit gates involving fSim gates. However, this ansatz does not yet satisfy constraint (3) and (4). Simply replacing the single  $R_z$

gate in the middle by a layer of  $R_z$  gate resolves this problem and leads to the final physics-constrained HEA, denoted by XYZ2F in Fig. 1b (with additional gates in blue). The size-consistency of XYZ2F can be seen as follows: Suppose the subsystems  $A$  and  $B$  contain the first two and the remaining two qubits, respectively, then the wavefunction  $|\Psi_A^L\rangle|\Psi_B^L\rangle$  formed by a direct product of the two XYZ2F wavefunctions can be represented by an XYZ2F ansatz for the composite system with  $U_{2,1} = I$  (see Fig. 1b). Therefore, the ability of  $U_2$  to become identity is essential from a size-consistent perspective, which is missing in other HEA shown in Fig. 1a. It can be verified that the constraint (4) is also satisfied by simply setting all  $U_2$  to identity, such that for the  $n$ -th qubit the circuit block gives a universal single-qubit gate

$$U = R_x(\theta_0)R_y(\theta_1)R_z(\theta_2)R_y^\dagger(\theta_1)R_x^\dagger(\theta_0). \quad (6)$$

In addition, the size-consistent modification also allows terms such as  $e^{i(\theta_1 X_0 X_1 + \theta_2 X_2 Z_3 Z_4 + \theta_3 Y_5)}$  to be implemented by a single layer in XYZ2F. In contrast,  $e^{i\theta_1 X_0 X_1} e^{i\theta_2 X_2 Z_3 Z_4} e^{i\theta_3 Y_5}$  needs to be implemented by three consecutive blocks in XYZ1F. This will greatly reduce the number of layers required to represent certain states, as will be shown numerically for the ground state of the Heisenberg model. In summary, the constructed physics-constrained HEA satisfies all the four fundamental constraints. The number of parameters in one layer of XYZ2F is  $(5N - 2)$ , where  $3N$  and  $2(N - 1)$  are for single-qubit and two-qubit gates, respectively. Comparing the exponential  $e^{i\theta_l P_l}$  with  $P_l \in \{I, X, Y, Z\}^{\otimes N}$ , it is seen that all the  $4^N$  discrete choices of  $P_l$  are now embedded into a continuous space of operators  $U_l(\vec{\theta}_l)$  specified by  $O(N)$  parameters.

## Numerical demonstration

We first use the one-dimensional Heisenberg model with open boundary condition, whose Hamiltonian is  $\hat{H} = -\frac{1}{2}J\sum_{n=1}^{N-1}\sigma_n \cdot \sigma_{n+1}$ , to study the effectiveness of the constructed HEA. To take full advantage of the systematic improvability of XYZ1F and XYZ2F, we use a layerwise optimization strategy (see Methods section). Figure 2 shows the convergence of the ground-state energy per site  $e_N^L$  obtained by different HEA for antiferromagnetic Heisenberg models as a function of the number of layers  $L$ , starting from a Néel state as reference  $|\Phi_0\rangle$ . We find that both XYZ1F and XYZ2F are systematically improvable as expected, and the effect of the size-consistent modification in XYZ2F is dramatic, which significantly

reduces the number of layers needed to reach certain accuracy. In contrast, other HEA do not converge monotonically and become increasingly difficult to converge as the system size  $N$  increases. As shown in Fig 2, the oscillatory behavior reveals a severe problem of these HEA in practical applications, that is, even if they have reached a certain accuracy with  $L$  layers, the accuracy with  $L + 1$  layers may be worse. The comparison with XYZ1F/XYZ2F suggests that it is the violation of constraints (2) and (3) that causes these heuristically designed HEA to perform poorly as  $N$  increases.

To further illustrate the size-consistency problem, we perform a size-consistent test<sup>51,53</sup> for different HEA in Table 1. We define a composite Heisenberg model (denoted by 6+6) consisting of two noninteracting subsystems with six sites. The parameters in the wavefunction of the composite system are taken from the optimized parameters for the subsystem. If an ansatz is size-consistent, then the ground-state energy per site  $e_N^L$  should be the same for the whole system and the subsystem, i.e.  $e_{6+6}^L = e_6^L$  for any  $L$ . Notably, only XYZ2F satisfies this condition, while other HEA violate it significantly. The additional entangling gates between subsystems in other HEA severely degrade the quality of the approximation in the total system, as can be seen from the significant increase of infidelity ( $1 - F_N^L$  with  $F_N^L = |\langle \Psi_N^L | \Psi_N^* \rangle|^2$ , where  $|\Psi_N^* \rangle$  is the exact wavefunction) in Table 1. In particular, the additional CNOT gates in the  $R_y$  full ansatz (see Fig. 1a) makes the fidelity between the approximate state and the ground state almost vanish. On the contrary, the infidelity for XYZ2F is well-controlled, that is, if the fidelity  $F_6^L$  is  $1 - \varepsilon$ , where  $\varepsilon$  is a small number (0.00085 for  $L = 2$  in Table 1), then the fidelity for the total system is  $(1 - \varepsilon)^2$ , and thus the infidelity  $1 - F_{6+6}^L$  is about  $2\varepsilon$ . Therefore, an interesting topic for future studies is to use parameters optimized from small systems as an initial guess of XYZ2F for large systems.

Finally, we examine the performance of the constructed HEA for realistic systems, including hydrogen chains ( $H_4$ ,  $H_6$ , and  $H_8$ ), LiH,  $H_2O$ , and  $N_2$ , which were commonly used to benchmark the performance of quantum computing techniques<sup>33,42,46,60</sup>. Figure 3 shows the convergence of the ground-state energy as a function of the number of layers  $L$ . We particularly focus on  $L$  required to achieve chemical accuracy (ca. 1 mH). For hydrogen chains, the number of Slater determinants with large coefficients in the expansion of the exact ground state increases significantly as the system size increases. As shown in Fig. 3, only XYZ2F converges monotonically to chemical accuracy, while other HEA perform poorly for  $H_6$  and  $H_8$ . The number of layers needed to achieve chemical accuracy increases approximately linearly with the



system size for XYZ2F. For LiH, H<sub>2</sub>O, and N<sub>2</sub>, all simulated with 12 qubits, the convergence behavior is quite different, reflecting the very different electronic structures. For LiH at  $R_{\text{Li-H}} = 2.0\text{\AA}$ , the exact ground state is dominated by the Hartree-Fock configuration (about 95%), and thus XYZ2F quickly reaches chemical accuracy with  $L = 3$ . For H<sub>2</sub>O and N<sub>2</sub> at stretched geometries upon dissociation, which are typical examples of strong electron correlations in quantum chemistry, the convergence is slower and the number of layers required for XYZ2F to reach chemical accuracy is 11 and 27, respectively. In comparison, we find that other HEA are difficult to converge to chemical accuracy for systems with more than ten qubits.

## Discussion

In this work, we introduced a new way to design HEA by satisfying fundamental constraints, inspired by the physics-constrained way to design non-empirical XC functionals in DFT<sup>48</sup>. The developed physics-constrained HEA - XYZ2F is superior to other heuristically designed HEA in terms of both accuracy and scalability. In particular, numerical tests show the promise of XYZ2F for challenging realistic molecules with strong electron correlation. The better scalability of XYZ2F is attributed to the satisfaction of the systematic improvability and size-consistency. Our results suggest that incorporating physical constraints into the design of HEA is a promising path towards designing efficient variational ansätze for solving many-body problems on quantum computers. It is conceivable that this work will inspire other realizations of HEA that satisfy these constraints, probably with more interesting properties such as less parameters, faster convergence, better trainability, and more versatile qubit connectivity.

## Methods

### Proof of Theorem 1

The proof of Theorem 1 in the main text is quite straightforward. Here we give two concrete examples in Fig. 4, arising from the double excitation  $a_0^\dagger a_2^\dagger a_4 a_5$  and the single excitation  $a_1^\dagger a_4$  in UCC, respectively. It can be easily verified that  $e^{i\theta Z_0 Z_1 Z_2 Z_4 Z_5}$  in Fig. 4a is given by XYZ1F in Fig. 4c with  $U_{2,k} = \text{CNOT}$  for  $k \in \{0, 1, 3, 4\}$  and  $U_{2,2} = \text{SWAP}/i\text{SWAP}$ , while  $e^{i\theta Z_1 Z_2 Z_3 Z_4}$  in Fig. 4b is given by  $U_{2,0} = I$ ,  $U_{2,k} = \text{CNOT}$  for  $k \in \{1, 2, 3\}$ , and  $U_{2,4} = \text{SWAP}/i\text{SWAP}$ . Other  $e^{i\theta P_l}$  can be represented by a similar recipe.

## Optimization strategy

To take advantage of the systematic improvability of XYZ1F and XYZ2F, the parameters in HEA are optimized in a layerwise way using the Algorithm 1. This is different from optimization with random initialization for all parameters, which has been shown to easily suffer from the problems of low-quality local minima and barren plateaus. Our algorithm has two key features: (1) we retain the optimized parameters from the previous step as the initial guess for the  $L - 1$  layers in the current step; (2) we generate  $n$  (about 10) sets of random parameters with different step sizes for the  $L$ -th layer. Each set of parameters  $\vec{\theta}_L$  is obtained from  $\vec{\theta}_L = \frac{\vec{u}}{\max_i |u_i|} \delta$ , where  $\vec{u}$  are random numbers in  $[-1, 1]$  and  $\delta$  is a predefined step size  $\delta \in \{\frac{2\pi}{2^k}\}_{k=0}^5 \cup \{0\}$ . This guarantees that the optimized energy decreases monotonically with respect to  $L$  for XYZ1F and XYZ2F.

---

### Algorithm 1 Layerwise optimization strategy

---

**Input:**  $L_{\max}, |\Phi_0\rangle$ ;

Initialization:  $L = 0, |\Psi\rangle = |\Phi_0\rangle$ ;

**while**  $L \leq L_{\max}$  **do**

Set  $L += 1$ ;

Generate  $n$  sets of random parameters  $\{\vec{\theta}_L^{(i)}\}_{i=1}^n$  with different step sizes for the  $L$ -th layer;

Combine  $\{\vec{\theta}_1, \dots, \vec{\theta}_{L-1}\}$  obtained in the previous step as initial guess for the  $L - 1$  layers;

Perform  $n$  independent VQE with  $|\Psi\rangle = U_L \cdots U_1 |\Phi_0\rangle$  in parallel;

Collect  $E_L = \min_i E_L^{(i)}$  and optimized  $\{\vec{\theta}_1, \dots, \vec{\theta}_L\}$ ;

**end while**

**Output:**  $\{E_1, \dots, E_{L_{\max}}\}$  and  $|\Psi\rangle = U_{L_{\max}} \cdots U_1 |\Phi_0\rangle$ .

---

## Computational details for molecules

For molecules, the molecular integrals were generated using the PySCF package<sup>61</sup> in a minimal STO-3G basis. The Jordan-Wigner fermion-to-qubit transformation<sup>62</sup> was carried out using OpenFermion<sup>63</sup>. Implementation of parameterized quantum circuits and automatic differentiation for energy gradients were performed with MindQuantum<sup>64</sup>. Numerical optimization in VQE employed the Broyden–Fletcher–Goldfarb–Shanno (BFGS) method implemented in Scipy<sup>65</sup>. For hydrogen chains, the orthonormalized atomic orbitals

(OAO) were used and the reference state was a Néel state, e.g.  $|\Phi_0\rangle = |10011001\rangle$  for  $H_4$ . For other molecules, the restricted Hartree-Fock (RHF) orbitals were used and the Hartree-Fock states are used as reference. For  $H_2O$ , the O1s orbital is frozen, while for  $N_2$  the N1s and N2s orbitals are frozen. We added a penalty term for particle number conservations in the calculation of  $H_2O$ , viz.  $\hat{H}' = \hat{H} + \beta(\hat{N}_\uparrow - n_\uparrow)^2 + \beta(\hat{N}_\downarrow - n_\downarrow)^2$  with  $\beta = 1.0$ . In the calculations of  $N_2$ , we further added a constraint for the total spin, viz.  $\hat{H}' = \hat{H} + \beta(\hat{N}_\uparrow - n_\uparrow)^2 + \beta(\hat{N}_\downarrow - n_\downarrow)^2 + \beta\hat{S}_+\hat{S}_-$  with  $\beta = 1.0$ .

## Date availability

All data supporting the findings of this study are available within the paper.

## Code availability

Source codes are available from the authors on request.

## References

1. Martin, R. M., Reining, L. & Ceperley, D. M. *Interacting electrons* (Cambridge University Press, 2016).
2. Gutzwiller, M. C. Effect of correlation on the ferromagnetism of transition metals. *Phys. Rev. Lett.* **10**, 159 (1963).
3. Jastrow, R. Many-body problem with strong forces. *Phys. Rev.* **98**, 1479 (1955).
4. White, S. R. Density matrix formulation for quantum renormalization groups. *Phys. Rev. Lett.* **69**, 2863 (1992).
5. Verstraete, F. & Cirac, J. I. Renormalization algorithms for quantum-many body systems in two and higher dimensions. *arXiv preprint cond-mat/0407066* (2004).
6. Shi, Y.-Y., Duan, L.-M. & Vidal, G. Classical simulation of quantum many-body systems with a tree tensor network. *Phys. Rev. A* **74**, 022320 (2006).
7. Vidal, G. Class of quantum many-body states that can be efficiently simulated. *Phys. Rev. Lett.* **101**, 110501 (2008).

8. Verstraete, F., Murg, V. & Cirac, J. I. Matrix product states, projected entangled pair states, and variational renormalization group methods for quantum spin systems. *Adv. Phys.* **57**, 143–224 (2008).
9. Schollwöck, U. The density-matrix renormalization group in the age of matrix product states. *Ann. Phys.* **326**, 96–192 (2011).
10. Orús, R. A practical introduction to tensor networks: Matrix product states and projected entangled pair states. *Ann. Phys.* **349**, 117–158 (2014).
11. Carleo, G. & Troyer, M. Solving the quantum many-body problem with artificial neural networks. *Science* **355**, 602–606 (2017).
12. Choo, K., Carleo, G., Regnault, N. & Neupert, T. Symmetries and many-body excitations with neural-network quantum states. *Phys. Rev. Lett.* **121**, 167204 (2018).
13. Liang, X. *et al.* Solving frustrated quantum many-particle models with convolutional neural networks. *Phys. Rev. B* **98**, 104426 (2018).
14. Choo, K., Neupert, T. & Carleo, G. Two-dimensional frustrated j 1- j 2 model studied with neural network quantum states. *Phys. Rev. B* **100**, 125124 (2019).
15. Hibat-Allah, M., Ganahl, M., Hayward, L. E., Melko, R. G. & Carrasquilla, J. Recurrent neural network wave functions. *Phys. Rev. Res.* **2**, 023358 (2020).
16. Sharir, O., Levine, Y., Wies, N., Carleo, G. & Shashua, A. Deep autoregressive models for the efficient variational simulation of many-body quantum systems. *Phys. Rev. Lett.* **124**, 020503 (2020).
17. Barrett, T. D., Malyshev, A. & Lvovsky, A. Autoregressive neural-network wavefunctions for ab initio quantum chemistry. *Nat. Mach. Intell.* **4**, 351–358 (2022).
18. Arute, F. *et al.* Quantum supremacy using a programmable superconducting processor. *Nature* **574**, 505–510 (2019).
19. Wu, Y. *et al.* Strong quantum computational advantage using a superconducting quantum processor. *Phys. Rev. Lett.* **127**, 180501 (2021).
20. Peruzzo, A. *et al.* A variational eigenvalue solver on a photonic quantum processor. *Nat. Commun.* **5**, 4213 (2014).

21. McClean, J. R., Romero, J., Babbush, R. & Aspuru-Guzik, A. The theory of variational hybrid quantum-classical algorithms. *New J. Phys.* **18**, 023023 (2016).
22. Tilly, J. *et al.* The variational quantum eigensolver: a review of methods and best practices. *Phys. Rep.* **986**, 1–128 (2022).
23. Cao, Y. *et al.* Quantum chemistry in the age of quantum computing. *Chem. Rev.* **119**, 10856–10915 (2019).
24. McArdle, S., Endo, S., Aspuru-Guzik, A., Benjamin, S. C. & Yuan, X. Quantum computational chemistry. *Rev. Mod. Phys.* **92**, 015003 (2020).
25. Bauer, B., Bravyi, S., Motta, M. & Chan, G. K.-L. Quantum algorithms for quantum chemistry and quantum materials science. *Chem. Rev.* **120**, 12685–12717 (2020).
26. Cerezo, M. *et al.* Variational quantum algorithms. *Nat. Rev. Phys.* **3**, 625–644 (2021).
27. Anand, A. *et al.* A quantum computing view on unitary coupled cluster theory. *Chem. Soc. Rev.* (2022).
28. Bartlett, R. J. & Musiał, M. Coupled-cluster theory in quantum chemistry. *Rev. Mod. Phys.* **79**, 291 (2007).
29. Preskill, J. Quantum computing in the nisq era and beyond. *Quantum* **2**, 79 (2018).
30. Whitfield, J. D., Biamonte, J. & Aspuru-Guzik, A. Simulation of electronic structure hamiltonians using quantum computers. *Mol. Phys.* **109**, 735–750 (2011).
31. Seeley, J. T., Richard, M. J. & Love, P. J. The bravyi-kitaev transformation for quantum computation of electronic structure. *J. Chem. Phys.* **137**, 224109 (2012).
32. Hastings, M. B., Wecker, D., Bauer, B. & Troyer, M. Improving quantum algorithms for quantum chemistry. *Quantum Inf. Comput.* **15**, 1–21 (2015).
33. Lee, J., Huggins, W. J., Head-Gordon, M. & Whaley, K. B. Generalized unitary coupled cluster wave functions for quantum computation. *J. Chem. Theory Comput.* **15**, 311–324 (2018).
34. Matsuzawa, Y. & Kurashige, Y. Jastrow-type decomposition in quantum chemistry for low-depth quantum circuits. *J. Chem. Theory Comput.* **16**, 944–952 (2020).

35. Ryabinkin, I. G., Yen, T.-C., Genin, S. N. & Izmaylov, A. F. Qubit coupled cluster method: a systematic approach to quantum chemistry on a quantum computer. *J. Chem. Theory Comput.* **14**, 6317–6326 (2018).
36. Grimsley, H. R., Economou, S. E., Barnes, E. & Mayhall, N. J. An adaptive variational algorithm for exact molecular simulations on a quantum computer. *Nat. Commun.* **10**, 3007 (2019).
37. Tang, H. L. *et al.* qubit-adapt-vqe: An adaptive algorithm for constructing hardware-efficient ansätze on a quantum processor. *PRX Quantum* **2**, 020310 (2021).
38. Yordanov, Y. S., Armaos, V., Barnes, C. H. & Arvidsson-Shukur, D. R. Qubit-excitation-based adaptive variational quantum eigensolver. *Commun. Phys.* **4**, 228 (2021).
39. Wecker, D., Bauer, B., Clark, B. K., Hastings, M. B. & Troyer, M. Gate-count estimates for performing quantum chemistry on small quantum computers. *Phys. Rev. A* **90**, 022305 (2014).
40. Wecker, D., Hastings, M. B. & Troyer, M. Progress towards practical quantum variational algorithms. *Phys. Rev. A* **92**, 042303 (2015).
41. Wiersema, R. *et al.* Exploring entanglement and optimization within the hamiltonian variational ansatz. *PRX Quantum* **1**, 020319 (2020).
42. Kandala, A. *et al.* Hardware-efficient variational quantum eigensolver for small molecules and quantum magnets. *Nature* **549**, 242 (2017).
43. Bittel, L. & Kliesch, M. Training variational quantum algorithms is np-hard. *Phys. Rev. Lett.* **127**, 120502 (2021).
44. Anschuetz, E. R. & Kiani, B. T. Quantum variational algorithms are swamped with traps. *Nat. Commun.* **13**, 7760 (2022).
45. McClean, J. R., Boixo, S., Smelyanskiy, V. N., Babbush, R. & Neven, H. Barren plateaus in quantum neural network training landscapes. *Nat. Commun.* **9**, 1–6 (2018).
46. D’Cunha, R., Crawford, T. D., Motta, M. & Rice, J. E. Challenges in the use of quantum computing hardware-efficient ansätze in electronic structure theory. *J. Phys. Chem. A* (2023).

47. Motta, M., Sung, K. J., Whaley, K. B., Head-Gordon, M. & Shee, J. Bridging physical intuition and hardware efficiency for correlated electronic states: the local unitary cluster jastrow ansatz for electronic structure. *ChemRxiv preprint ChemRxiv:10.26434/chemrxiv-2023-d1b3l* (2023).
48. Kaplan, A. D., Levy, M. & Perdew, J. P. The predictive power of exact constraints and appropriate norms in density functional theory. *Annu. Rev. Phys. Chem.* **74**, 193–218 (2023).
49. Perdew, J. P., Burke, K. & Ernzerhof, M. Generalized gradient approximation made simple. *Phys. Rev. Lett.* **77**, 3865 (1996).
50. Sun, J., Ruzsinszky, A. & Perdew, J. P. Strongly constrained and appropriately normed semilocal density functional. *Phys. Rev. Lett.* **115**, 036402 (2015).
51. Pople, J. A., Binkley, J. S. & Seeger, R. Theoretical models incorporating electron correlation. *Int. J. Quantum Chem.* **10**, 1–19 (1976).
52. Bartlett, R. J. Many-body perturbation theory and coupled cluster theory for electron correlation in molecules. *Annu. Rev. Phys. Chem.* **32**, 359–401 (1981).
53. Nooijen, M., Shamasundar, K. & Mukherjee, D. Reflections on size-extensivity, size-consistency and generalized extensivity in many-body theory. *Mol. Phys.* **103**, 2277–2298 (2005).
54. Nielsen, M. A. & Chuang, I. L. *Quantum computation and quantum information* (Cambridge University Press, 2010).
55. Evangelista, F. A., Chan, G. K.-L. & Scuseria, G. E. Exact parameterization of fermionic wave functions via unitary coupled cluster theory. *The J. chemical physics* **151**, 244112 (2019).
56. Kjaergaard, M. *et al.* Superconducting qubits: Current state of play. *Annu. Rev. Condens. Matter Phys.* **11**, 369–395 (2020).
57. Vidal, G. & Dawson, C. M. Universal quantum circuit for two-qubit transformations with three controlled-not gates. *Phys. Rev. A* **69**, 010301 (2004).
58. Vatan, F. & Williams, C. Optimal quantum circuits for general two-qubit gates. *Phys. Rev. A* **69**, 032315 (2004).

59. Foxen, B. *et al.* Demonstrating a continuous set of two-qubit gates for near-term quantum algorithms. *Phys. Rev. Lett.* **125**, 120504 (2020).
60. Arute, F. *et al.* Hartree-fock on a superconducting qubit quantum computer. *Science* **369**, 1084–1089 (2020).
61. Sun, Q. *et al.* Pyscf: the python-based simulations of chemistry framework. *Wiley Interdiscip. Rev. Comput. Mol. Sci.* **8**, e1340 (2018).
62. Jordan, P. & Wigner, E. About the pauli exclusion principle. *Z. Phys.* **47**, 631 (1928).
63. McClean, J. R. *et al.* Openfermion: the electronic structure package for quantum computers. *Quantum Sci. Technol.* **5**, 034014 (2020).
64. MindQuantum Developer. Mindquantum, version 0.6.0 (2021).
65. Virtanen, P. *et al.* Scipy 1.0: fundamental algorithms for scientific computing in python. *Nat. Methods* **17**, 261–272 (2020).

## Acknowledgements

This work was supported by the National Natural Science Foundation of China (Grants No. 21973003) and the Fundamental Research Funds for the Central Universities.

## Author contributions

X.X. and Z.L. conceived the study. X.X. and H.Z. carried out numerical calculations. All authors X.X., H.Z., J.R., W.F., and Z.L. discussed the results and contributed to the writing of the manuscript.

## Competing interests

The authors declare no competing interests.



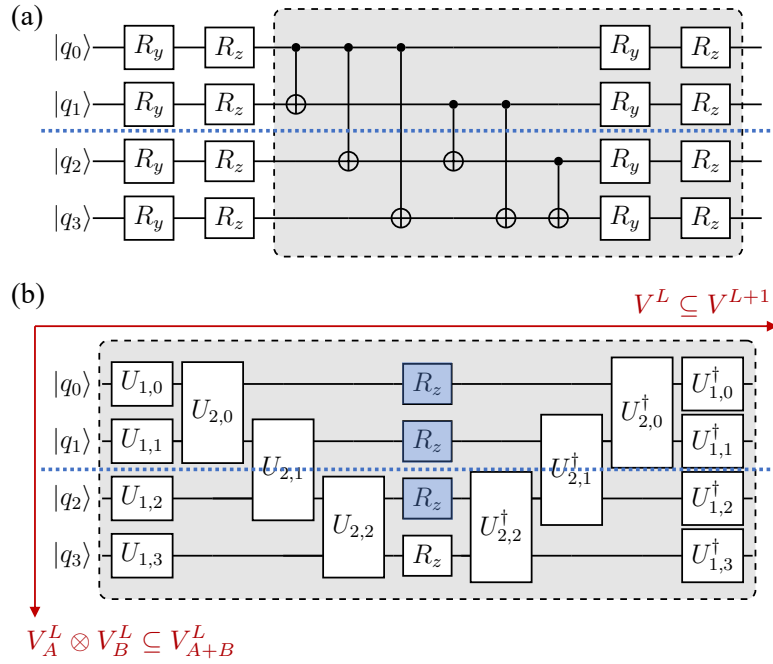


**Figure 1.** Heuristically designed HEA and physics-constrained HEA. (a)  $R_y R_z$  full (EfficientSU2) ansatz. The  $R_y$  full ansatz can be obtained by removing the columns of  $R_z$  gates, while the  $R_y$  linear ansatz can be derived from the  $R_y$  full ansatz by further replacing the all-to-all CNOT gates by nearest neighbor CNOT gates. (b) XYZ1F (gates in white) and XYZ2F (gates in white and blue) ansätze. The dashed box indicates a single repeating unit  $U_l(\vec{\theta}_l)$ , and all the parameters are omitted for brevity. The two inclusion constraints  $V^L \subseteq V^{L+1}$  and  $V_A^L \otimes V_B^L \subseteq V_{A+B}^L$  for extending HEA in different directions of quantum circuits are highlighted. The blue dashed line represents a partition of the whole system into two subsystems  $A$  and  $B$ .

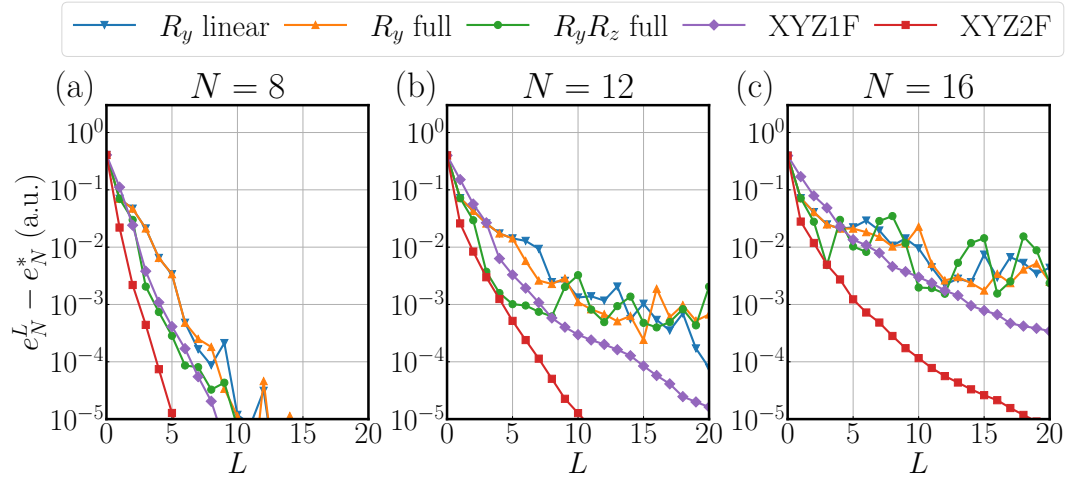


**Figure 2.** Convergence of the ground-state energy per site  $e_N^L$  obtained by different HEA ( $R_y$  linear,  $R_y$  full,  $R_y R_z$  full, XYZ1F and XYZ2F) as a function of the number of layers  $L$  for one-dimensional antiferromagnetic Heisenberg models ( $J = -1$ ) with  $N$  sites ( $N = 8, 12$ , and  $16$ ). The exact values  $e_N^*$  are obtained from exact diagonalizations. While both XYZ1F and XYZ2F are systematically improvable, the size-consistency of XYZ2F makes it superior to XYZ1F. Other HEA do not converge monotonically, and become increasingly difficult to achieve a target accuracy as the system size increases.

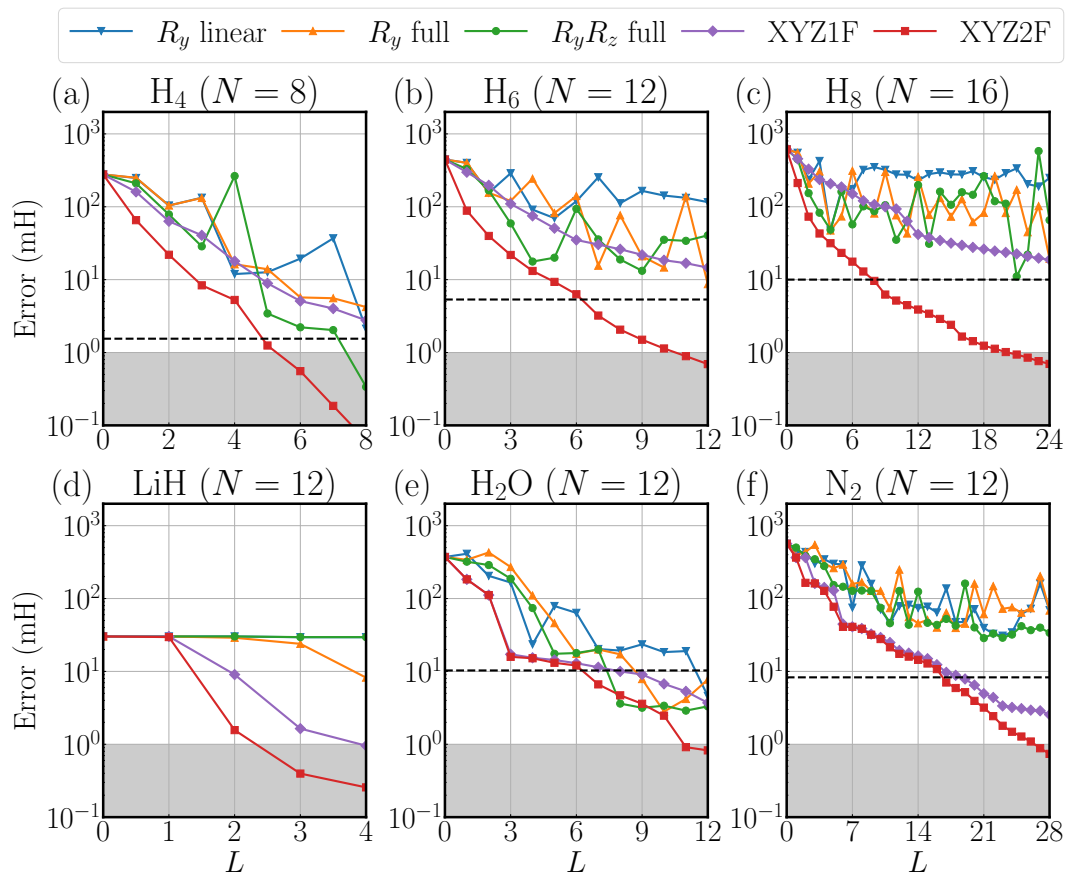


**Figure 3.** Ground-state energy convergence with respect to exact diagonalization results as a function of the number of layers  $L$  for molecules: (a)-(c) hydrogen chains ( $H_4$ ,  $H_6$ , and  $H_8$ ) with interatomic distance  $R_{H-H} = 1.5$  Å; (d)  $LiH$  ( $R_{Li-H} = 2.0$  Å); (e)  $H_2O$  ( $R_{O-H} = 2.0$  Å and  $\theta_{H-O-H} = 104.5$  degree); (f)  $N_2$  ( $R_{N-N} = 2.0$  Å). For more computational details, see Methods section. The black dashed lines represent UCCSD results, while the shaded regions represent the region within chemical accuracy (1 mH).

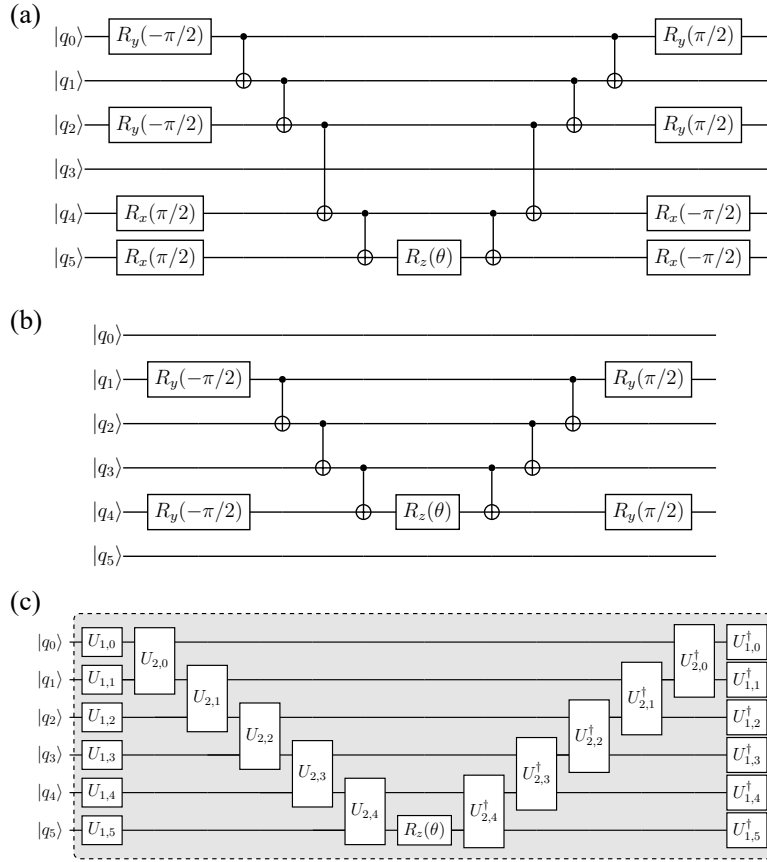


**Figure 4.** Examples for Theorem 1 with six qubits. (a),(b) quantum circuits appeared in UCC arising from the double excitation  $a_0^\dagger a_2^\dagger a_4 a_5$  and the single excitation  $a_1^\dagger a_4$ , respectively; (c) the XYZ1F circuit. Both (a) and (b) can be represented by (c) by appropriately choosing single-qubit gates  $U_{1,k}$  from  $\{I, R_x(\pi/2), R_y(-\pi/2) \text{ or } H\}$  and two-qubit gates  $U_{2,k}$  from  $\{I, \text{CNOT}, \text{SWAP} \text{ or } \text{iSWAP}\}$ .

**Table 1.** Size-consistency test: ground-state energy per site  $e_N^L$  and infidelities ( $1 - F_N^L$  with  $F_N^L = |\langle \Psi_N^L | \Psi_N^* \rangle|^2$ ) obtained by different HEA with  $L = 2$  and  $L = 4$  for a composite Heisenberg model (denoted by 6+6), which consists of two noninteracting subsystems with six sites. The parameters of the total system are taken from the optimized parameters of the subsystems. Errors with respect to the exact  $e_N^*$  obtained from exact diagonalization are shown in parenthesis. Only XYZ2F satisfies  $e_{6+6}^L = e_6^L$ , while other HEA are not size-consistent.

system	$R_y$ linear	$R_y$ full	$R_y R_z$ full	XYZ2F
$e_6^{L=2}$	-0.78333 (0.04786)	-0.78333 (0.04786)	-0.80606 (0.02514)	-0.83054 ( <b>0.00065</b> )
$e_{6+6}^{L=2}$	-0.52002 (0.31118)	-0.51368 (0.31751)	-0.64791 (0.18328)	-0.83054 ( <b>0.00065</b> )
$e_6^{L=4}$	-0.82988 (0.00132)	-0.82988 (0.00132)	-0.83089 (0.00030)	-0.83119 ( <b>0.00000</b> )
$e_{6+6}^{L=4}$	-0.33247 (0.49873)	-0.35020 (0.48099)	-0.53154 (0.29966)	-0.83119 ( <b>0.00000</b> )
$1 - F_6^{L=2}$	0.17623	0.17623	0.03743	<b>0.00085</b>
$1 - F_{6+6}^{L=2}$	0.77773	1.00000	1.00000	<b>0.00170</b>
$1 - F_6^{L=4}$	0.00205	0.00205	0.00037	<b>0.00000</b>
$1 - F_{6+6}^{L=4}$	0.93368	1.00000	0.93196	<b>0.00000</b>